International Journal of Thermal Sciences 49 (2010) 479–491

Contents lists available at ScienceDirect

International Journal of Thermal Sciences

journal homepage: www.elsevier.com/locate/ijts

Effect of nanofluid variable properties on natural convection in enclosures

Eiyad Abu-Nada [a,b,c,*], Ziyad Masoud [c], Hakan F. Oztop [d], Antonio Campo [e]

[a] Department of Mechanical Engineering and Applied Mechanics, University of Rhode Island, 92 Upper College Rd., Kingston, RI 02881, USA
[b] Leibniz Universtät Hannover, Institute für Technishe Verbrennung, Welfengarten 1a, 30167 Hannover, Germany
[c] Department of Mechanical Engineering, Hashemite University, Zarqa 13115, Jordan
[d] Department of Mechanical Education, Fırat University, Elazig TR-23119, Turkey
[e] Department of Mechanical Engineering, The University of Texas at San Antonio, San Antonio, TX 78249, USA

ARTICLE INFO

Article history:
Received 21 March 2009
Received in revised form
21 July 2009
Accepted 6 September 2009
Available online 2 October 2009

Keywords:
Nanofluid
Viscosity
Thermal conductivity
Natural convection
Enclosure

ABSTRACT

In this work, the heat transfer enhancement in a differentially heated enclosure using variable thermal conductivity and variable viscosity of Al_2O_3–water and CuO–water nanofluids is investigated. The results are presented over a wide range of Rayleigh numbers ($Ra = 10^3$–10^5), volume fractions of nanoparticles ($0 \le \varphi \le 9\%$), and aspect ratios ($½ \le A \le 2$). For an enclosure with unity aspect ratio, the average Nusselt number of a Al_2O_3–water nanofluid at high Rayleigh numbers was reduced by increasing the volume fraction of nanoparticles above 5%. However, at low Rayleigh numbers, the average Nusselt number was slightly enhanced by increasing the volume fraction of nanoparticles. At high Rayleigh numbers, CuO–water nanofluids manifest a continuous decrease in Nusselt number as the volume fraction of nanoparticles is increased. However, the Nusselt number was not sensitive to the volume fraction at low Rayleigh numbers. The Nusselt number demonstrates to be sensitive to the aspect ratio. It was observed that enclosures, having high aspect ratios, experience more deterioration in the average Nusselt number when compared to enclosures having low aspect ratios. The variable thermal conductivity and variable viscosity models were compared to both the Maxwell-Garnett model and the Brinkman model. It was found that at high Rayleigh numbers the average Nusselt number was more sensitive to the viscosity models than to the thermal conductivity models.

1. Introduction

Natural convection heat transfer is an important phenomenon in engineering systems due to its wide applications in electronics cooling, heat exchangers, and double pane windows [1–4]. Enhancement of heat transfer in these systems is essential from the industrial and energy saving perspectives. The low thermal conductivity of conventional heat transfer fluids, such as water, is considered a primary limitation on the performance and the compactness of thermal systems. An innovative technique for the improvement of heat transfer using nanoscale particles dispersed in a base fluid, known as nanofluid, has been studied extensively during the recent years [5–7], especially for forced convection applications. On the contrary, natural convection heat transfer research using nanofluids is scarce and has received very little attention. In view of this, there is still a debate on the role that nanoparticles play on the heat transfer enhancement in natural convection applications.

Examples of controversial results are found in the results reported by Khanafer et al. [8] who studied Cu–water nanofluids in a two-dimensional rectangular enclosure. These authors reported an augmentation in heat transfer with an increment percentage of the suspended nanoparticles at any given Grashof number. Oztop and Abu-Nada [9] showed similar results, where an enhancement in heat transfers was registered by the addition of nanoparticles. However, contradictory experimental findings were reported by Putra et al. [10] using Al_2O_3 and CuO water nanofluids. These authors found that the natural convection heat transfer coefficient was lower than that for a clear fluid. Moreover, another experimental work in natural convection conducted by Wen and Ding [11], highlighted deterioration in heat transfer by the addition of nanoparticles. Most recently, Abu-Nada et al. [12] demonstrated that the enhancement of heat transfer in natural convection depends mainly on the magnitude of Rayleigh number. In fact, for a certain Rayleigh number, like $Ra = 10^4$, the heat transfer was not sensitive to nanoparticles, whereas at higher values of Rayleigh number, an enhancement in heat transfer was observed. Therefore, there is still a controversy on the role of nanofluids in natural convection heat transfer where the numerical simulations seem to over estimate the level of enhancement.

* Corresponding author. Tel.: +962 390 3333; fax: +962 382 6613.
E-mail address: eiyad@hu.edu.jo (E. Abu-Nada).

1290-0729/$ – see front matter © 2009 Elsevier Masson SAS. All rights reserved.
doi:10.1016/j.ijthermalsci.2009.09.002

Nomenclature

A	aspect ratio (W/H)
C_p	specific heat at constant pressure (kJ kg^{-1} K^{-1})
d	diameter (m)
g	gravitational acceleration (m s^{-2})
H	height of the enclosure (m)
h	local heat transfer coefficient (W m^{-2} K^{-1})
k	thermal conductivity (W m^{-1} K^{-1})
Nu	Nusselt number, $Nu = hH/k_f$
Pr	Prandtl number, $Pr = \nu_{f_o}/\alpha_{f_o}$
q_w	heat flux (W m^{-2})
Ra	Rayleigh number, $Ra = g\beta(T_H - T_L)H^3/\nu_{f_o}\alpha_{f_o}$
Re	Reynolds number, $Re = \rho_f k_b T/3\pi\mu_f^2 l_f$
T	dimensional temperature (°C)
u, v	dimensional x and y-components of velocity (m s^{-1})
U, V	dimensionless velocities, $V = vH/\alpha_f U = uH/\alpha_f$
W	width of the enclosure (m)
x, y	dimensionless coordinates, $x = x'/Hy = y'/H$
x', y'	dimensional coordinates (m)

Greek symbols

α	fluid thermal diffusivity (m^2 s^{-1})
β	thermal expansion coefficient (K^{-1})
ε	numerical tolerance
φ	nanoparticle volume fraction
ν	kinematic viscosity (m^2 s^{-1})
θ	dimensionless temperature, $\theta = (T - T_C)/(T_H - T_C)$
ψ	dimensional stream function (m^2 s^{-1})
Ψ	dimensionless stream function, $\Psi = \psi/\alpha_f$
ω	dimensional vorticity (s^{-1})
Ω	dimensionless vorticity, $\Omega = \omega H^2/\alpha_f$
ρ	density (kg m^{-3})
μ	dynamic viscosity (N s m^{-2})

Subscripts

avg	average
C	cold
f	fluid
H	hot
nf	nanofluid
p	particle
w	wall

Conceptually, natural convection heat transfer is affected by nanofluid properties such as viscosity and thermal conductivity. All of the previously mentioned numerical works relied on the Brinkman model for the viscosity. This model tends to underestimate the effective viscosity of the nanofluid as stated by Pak and Cho [13] and Nguyen et al. [14]. The Brinkman model does not consider the effect of nanofluid temperature or nanoparticles size. Moreover, the model was derived for particles that are much larger than the nanoscale size of the nanoparticles. In this context, Polidori et al. [15] concluded that the heat transfer was not only characterized by nanofluid thermal conductivity. They added that viscosity also plays a major role in the heat transfer behavior.

On the other hand, most of the above-mentioned numerical simulations available in the literature used the Maxwell-Garnett (MG) model for the thermal conductivity. This model does not account for important mechanisms for heat transfer in nanofluids such as Brownian motion. Owing to this deficiency, numerical simulations need to incorporate more robust models for the viscosity and thermal conductivity that take into account both the temperature dependence and the nanoparticle size. Recently, Nguyen et al. [14] and Angue Minsta et al. [16] studied experimentally the effect nanoparticles concentration and nanoparticles size on nanofluids viscosity under a wide range of temperatures. They infer that viscosity drops sharply with temperature especially for high concentration of nanoparticles. Moreover, the combined effect of temperature, nanoparticle size, and nanoparticles volume fraction on the thermal conductivity of nanofluids was studied experimentally by Chon et al. [17]. Therefore, it is obvious that the dependence of nanofluid properties on temperature, volume fraction of nanoparticles, must be accounted in order to predict the correct contribution of nanoparticles to the heat transfer enhancement. Abu-Nada [18], recently studied the effect of variable properties of Al_2O_3–water nanofluids on natural convection in an annular region. He found that the heat transfer was elevated by increasing the concentration of nanoparticles for $Ra \geq 10^4$. However, there was an enhancement in heat transfer at $Ra = 10^3$. Therefore, the scope of the current work to extend the outcome of this research to examine the sensitivity of natural convection heat transfer to variable viscosity and thermal conductivity of nanofluids in differentially heated enclosures. The work will focus on two types of nanofluids, namely Al_2O_3–water nanofluid and CuO–water nanofluid. The detailed experimental results reported by Nguyen et al. [14] will be used to derive a correlation for nanofluids viscosity as a function of temperature and nanoparticles concentration. Also, the model derived by Chon et al. [17] will be adopted for the thermal conductivity. This work will evaluate the impact of both variable viscosity and variable thermal conductivity, derived from experimental data, on heat transfer in natural convection in a differentially heated enclosure. The enhancement in heat transfer will be evaluated under a wide range of operating temperatures and a wide range of volume fraction of nanoparticles.

2. Governing equations and problem formulation

Fig. 1 is a schematic diagram of a differentially heated enclosure. The height and the width of the enclosure are given by H and W, respectively. The left wall is heated and maintained at a constant temperature (T_H) higher than the right cold wall temperature (T_C).

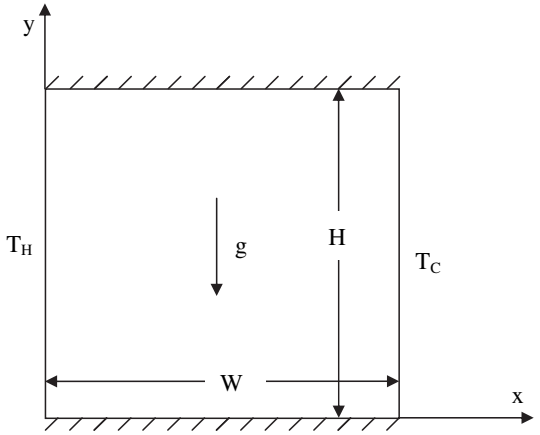

Fig. 1. Schematic of the enclosure.

The fluid in the enclosure is a water-based nanofluid containing Al_2O_3 or CuO nanoparticles. The nanofluid is assumed incompressible and the flow is conceived as laminar and two-dimensional. It is idealized that water and nanoparticles are in thermal equilibrium and no slip occurs between the two media. The thermo-physical properties of the nanofluid are listed in Table 1 [18,19]. The density of the nanofluid is approximated by the standard Boussinesq model. The viscosity and the thermal conductivity of the nanofluid are considered as variable properties; both vary with temperature and volume fraction of nanoparticles.

The governing equations for the laminar, steady state natural convection in terms of the stream function-vorticity formulation are given as:

Vorticity

$$\frac{\partial}{\partial x'}\left(\omega\frac{\partial\psi}{\partial y'}\right)-\frac{\partial}{\partial y'}\left(\omega\frac{\partial\psi}{\partial x'}\right)=\frac{1}{\rho_{nf}}\left(\frac{\partial}{\partial x'}\left[\mu_{nf}\frac{\partial\omega}{\partial x'}\right]+\frac{\partial}{\partial y'}\left[\mu_{nf}\frac{\partial\omega}{\partial y'}\right]\right)+(\varphi\beta_p+(1-\varphi)\beta_f)g\left(\frac{\partial T}{\partial x'}\right) \quad (1)$$

Energy

$$\frac{\partial}{\partial x'}\left(T\frac{\partial\psi}{\partial y'}\right)-\frac{\partial}{\partial y'}\left(T\frac{\partial\psi}{\partial x'}\right)=\frac{\partial}{\partial x'}\left[\alpha_{nf}\frac{\partial T}{\partial x'}\right]+\frac{\partial}{\partial y'}\left[\alpha_{nf}\frac{\partial T}{\partial y'}\right] \quad (2)$$

Kinematics

$$\frac{\partial^2\psi}{\partial x'^2}+\frac{\partial^2\psi}{\partial y'^2}=-\omega \quad (3)$$

The horizontal and vertical velocities are given by the following relations:

$$u=\frac{\partial\psi}{\partial y'} \quad (4)$$

$$v=-\frac{\partial\psi}{\partial x'} \quad (5)$$

In Eqs. (1) and (2), the thermal diffusivity is written as:

$$\alpha_{nf}=\frac{k_{nf}}{(\rho c_p)_{nf}} \quad (6)$$

Also, the effective density of the nanofluid is given by:

$$\rho_{nf}=(1-\varphi)\rho_f+\varphi\rho_p \quad (7)$$

The heat capacitance of the nanofluid is expressed as:

$$(\rho c_p)_{nf}=(1-\varphi)(\rho c_p)_f+\varphi(\rho c_p)_p \quad (8)$$

The effective thermal conductivity of the nanofluid calculated by the Chon et al. model [17] is:

$$\frac{k_{nf}}{k_f}=1+64.7\varphi^{0.7640}\left(\frac{d_f}{d_p}\right)^{0.3690}\left(\frac{k_f}{k_p}\right)^{0.7476}Pr_T^{0.9955}Re^{1.2321} \quad (9)$$

Table 1
Thermo-physical properties of fluid and nanoparticles [18,19].

Physical properties	Fluid phase (water)	Al_2O_3	CuO
C_p (J/kg K)	4179	765	540
ρ (kg/m^3)	997.1	3970.	6500
k (W m^{-1} K^{-1})	0.613	25.	18.0
$\beta\times10^{-5}$ (1/K)	21	0.85	0.85
d_p (nm)	0.384	47	29

Here Pr_T and Re are defined by:

$$Pr_T=\frac{\mu_f}{\rho_f\alpha_f} \quad (10)$$

$$Re=\frac{\rho_f k_b T}{3\pi\mu_f^2 l_f} \quad (11)$$

The symbol k_b is the Boltzmann constant $= 1.3807\times10^{-23}$ J/K, and l_f is the mean path of fluid particles given as 0.17 nm [17]. This model embraces the effect of nanoparticle size and temperature on nanofluid thermal conductivity encompassing a wide temperature range between 21 and 70 °C. It is also worth emphasizing that this model is based on experimental measurements of Al_2O_3 nanoparticles in water for volume fractions up to 4%. However, this model was tested experimentally by Angue Minsta et al. [16] for the pair of Al_2O_3 and CuO nanoparticles and found suitable to predict the thermal conductivity of these nanoparticles up to a volume fraction of 9%. The results using Eq. (9) will be compared to the MG model given by [9,12]:

$$\frac{k_{nf}}{k_f}=\frac{k_p+(n-1)k_f-(n-1)(k_f-k_p)\varphi}{k_p+(n-1)k_f+(k_f-k_p)\varphi} \quad (12)$$

where $n=3$. The correlation for the dynamic viscosity of Al_2O_3–water nanofluid is derived using available experimental data of Nguyen et al. [14]. In fact, no explicit correlation is given in Nguyen et al. [14] that define the viscosity of Al_2O_3–water nanofluid as a double function of temperature and volume fraction of nanoparticles simultaneously. Therefore, in the present work, such a correlation was derived based on the two-dimensional regression analysis performed on the experimental data of Nguyen et al. [14]. The R^2 value is 99.8% and a maximum error is 5%. The correlations for Al_2O_3 and CuO nanofluids are defined, respectively by:

$$\mu_{Al_2O_3}(c_p)=\exp(3.003-0.04203T-0.5445\varphi+0.0002553T^2+0.0524\varphi^2-1.622\varphi^{-1}) \quad (13)$$

$$\mu_{CuO}(c_p)=-0.6967+\left(\frac{15.937}{T}\right)+1.238\varphi+\left(\frac{1356.14}{T^2}\right)-.259\varphi^2-30.88\left(\frac{\varphi}{T}\right)-\left(\frac{19652.74}{T^3}\right)+.01593\varphi^3+4.38206\left(\frac{\varphi^2}{T}\right)+147.573\left(\frac{\varphi}{T^2}\right) \quad (14)$$

The viscosity in Eqs. (13) and (14) is expressed in centi poise and the temperature in °C. Fig. 2 presents a plot of the viscosity of Al_2O_3–water and CuO–water nanofluids as a function of temperature and concentration of nanoparticles calculated using Eqs. (13) and (14). The figure also shows the measured data from Nguyen et al. experiments [14]. It is very clear that the current nonlinear regression is in good agreement with the experimental measurements. In the discussion section, the results, using Eqs. (13) and (14) will be compared to the Brinkman model given by [9,12]:

$$\mu_{nf}=\frac{\mu_f}{(1-\varphi)^{2.5}} \quad (15)$$

It is worth mentioning that the viscosity of the base fluid (water) is considered to vary with temperature and the flowing equation is used to evaluate the viscosity of water,

$$\mu_{H_2O}(c_p)=-81.1+98.75\ln(T)-45.23\ln^2(T)+9.71\ln^3(T)-0.946\ln^4(T)+0.03\ln^5(T) \quad (16)$$

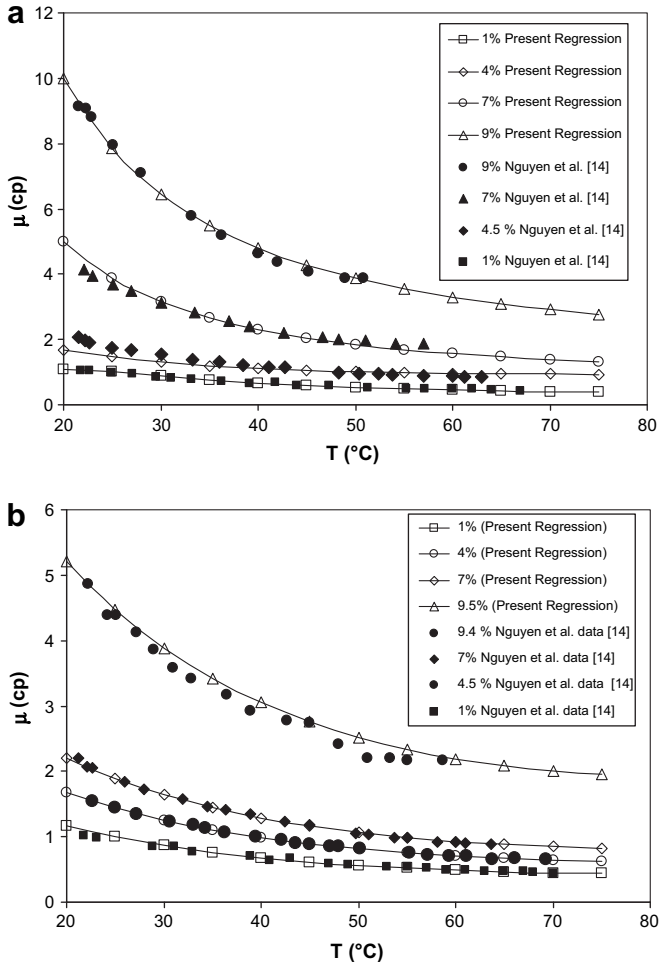

Fig. 2. (a) Comparison between CuO–water viscosities calculated using Eq. (14) and those of reference [14]. (b) Comparison between Al_2O_3–water viscosities calculated using Eq. (13) and those of reference [14].

The following dimensionless variables are introduced:

$$x = \frac{x'}{H};\quad y = \frac{y'}{H};\quad \Omega = \frac{\omega}{\alpha_{f_o}/H^2};\quad \Psi = \frac{\psi}{\alpha_{f_o}};\quad V = \frac{v}{\alpha_{f_o}/H};$$

$$U = \frac{u}{\alpha_{f_o}/H};\quad \theta = \frac{T - T_C}{T_H - T_C}$$

$$k = \frac{k_{nf}}{k_{f_o}},\quad \alpha = \frac{\alpha_{nf}}{\alpha_{f_o}},\quad \mu = \frac{\mu_{nf}}{\mu_{f_o}} \tag{17}$$

where the subscript "o" stands for the reference temperature which is taken as 22 °C in the current study. The aspect ratio (A) is defined as the ratio of width to the height of the enclosure ($A = W/H$).

The governing equations are re-written in dimensionless form as:

$$\frac{\partial}{\partial x}\left(\Omega\frac{\partial\Psi}{\partial y}\right) - \frac{\partial}{\partial y}\left(\Omega\frac{\partial\Psi}{\partial x}\right) = \frac{Pr}{(1-\varphi)+\varphi\frac{\rho_p}{\rho_f}}\left(\frac{\partial}{\partial x}\left(\mu\frac{\partial\Omega}{\partial x}\right) + \frac{\partial}{\partial y}\left(\mu\frac{\partial\Omega}{\partial y}\right)\right) + Ra\,Pr\left(\varphi\left(\frac{\beta_p}{\beta_f}\right) + (1-\varphi)\right)\left(\frac{\partial\theta}{\partial x}\right) \tag{18}$$

Table 2
Comparison of average Nusselt number with other published data for $Pr = 0.7$.

	$Ra = 10^3$	$Ra = 10^4$	$Ra = 10^5$	$Ra = 10^6$
Present work	1.120	2.244	4.644	8.862
De Vahl Davis [1]	1.118	2.243	4.520	8.799
Barakos and Mistoulis [2]	1.114	2.245	4.510	8.806
Fusegi et al. [3]	1.105	2.230	4.646	9.012
Khanafer et al. [8]	1.118	2.245	4.522	8.826

$$\frac{\partial}{\partial x}\left(\theta\frac{\partial\Psi}{\partial y}\right) - \frac{\partial}{\partial y}\left(\theta\frac{\partial\Psi}{\partial x}\right) = \frac{1}{(1-\varphi)+\varphi\frac{(\rho c_p)_p}{(\rho c_p)_f}} \times\left[\frac{\partial}{\partial x}\left(k\frac{\partial\theta}{\partial x}\right) + \frac{\partial}{\partial y}\left(k\frac{\partial\theta}{\partial y}\right)\right] \tag{19}$$

$$\frac{\partial^2\Psi}{\partial x^2} + \frac{\partial^2\Psi}{\partial y^2} = -\Omega \tag{20}$$

where the dimensionless numbers are

$$Ra = \frac{g\beta(T_H - T_L)H^3}{\nu_{f_o}\alpha_{f_o}} \tag{21}$$

$$Pr = \frac{\nu_{f_o}}{\alpha_{f_o}} \tag{22}$$

The dimensionless horizontal and vertical velocities are converted to:

$$U = \frac{\partial\Psi}{\partial y} \tag{23}$$

$$V = -\frac{\partial\Psi}{\partial x} \tag{24}$$

The dimensionless boundary conditions can be written as:

$$1 - \text{On the left wall i.e., } x = 0,\ \Psi = 0,\quad \Omega = -\frac{\partial^2\Psi}{\partial x^2},\quad \theta = 1$$

$$2 - \text{On the right wall i.e., } x = 1,\ \Psi = 0,\quad \Omega = -\frac{\partial^2\Psi}{\partial x^2},\quad \theta = 0.$$

$$3 - \text{On the top and bottom walls : } \Psi = 0,\ \Omega = -\frac{\partial^2\Psi}{\partial y^2},\quad \frac{\partial\theta}{\partial y} = 0 \tag{25}$$

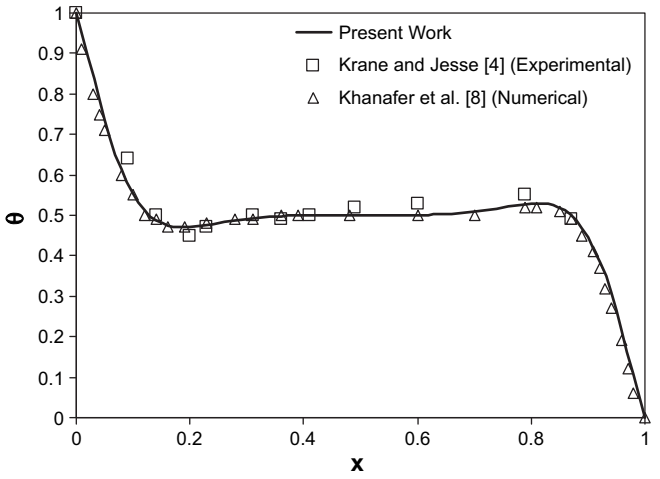

Fig. 3. Comparison between present work and other published data for the temperature distribution at the vertical mid section along the width of the enclosure ($Ra = 10^5$, $Pr = 0.7$).

3. Numerical implementation

Equations (18) through (20), absorbing the variable properties given in Eqs. (9), (13) and (14) along with the corresponding boundary conditions given in Eq. (25) are solved using a finite volume method [20,21]. The diffusion term in the vorticity and energy equations is approximated by a second-order central difference scheme which is conducive to a stable solution. Furthermore, a second-order upwind differencing scheme is adopted for the convective terms. For full details of the numerical implementation, the reader is referred to Oztop and Abu-Nada [9].

After solving for Ψ, Ω, and θ, more useful quantities for engineering applications are obtained. For example, the Nusselt number can be expressed as:

$$Nu = \frac{hH}{k_f} \tag{26}$$

The heat transfer coefficient is computed from:

$$h = \frac{q_w}{T_H - T_L} \tag{27}$$

The thermal conductivity of the nanofluid is defined by:

$$k_{nf} = -\frac{q_w}{\partial T/\partial x} \tag{28}$$

Substituting Eqs. (27) and (28) into Eq. (26), and using the dimensionless quantities, the local Nusselt number along the left wall can be written as:

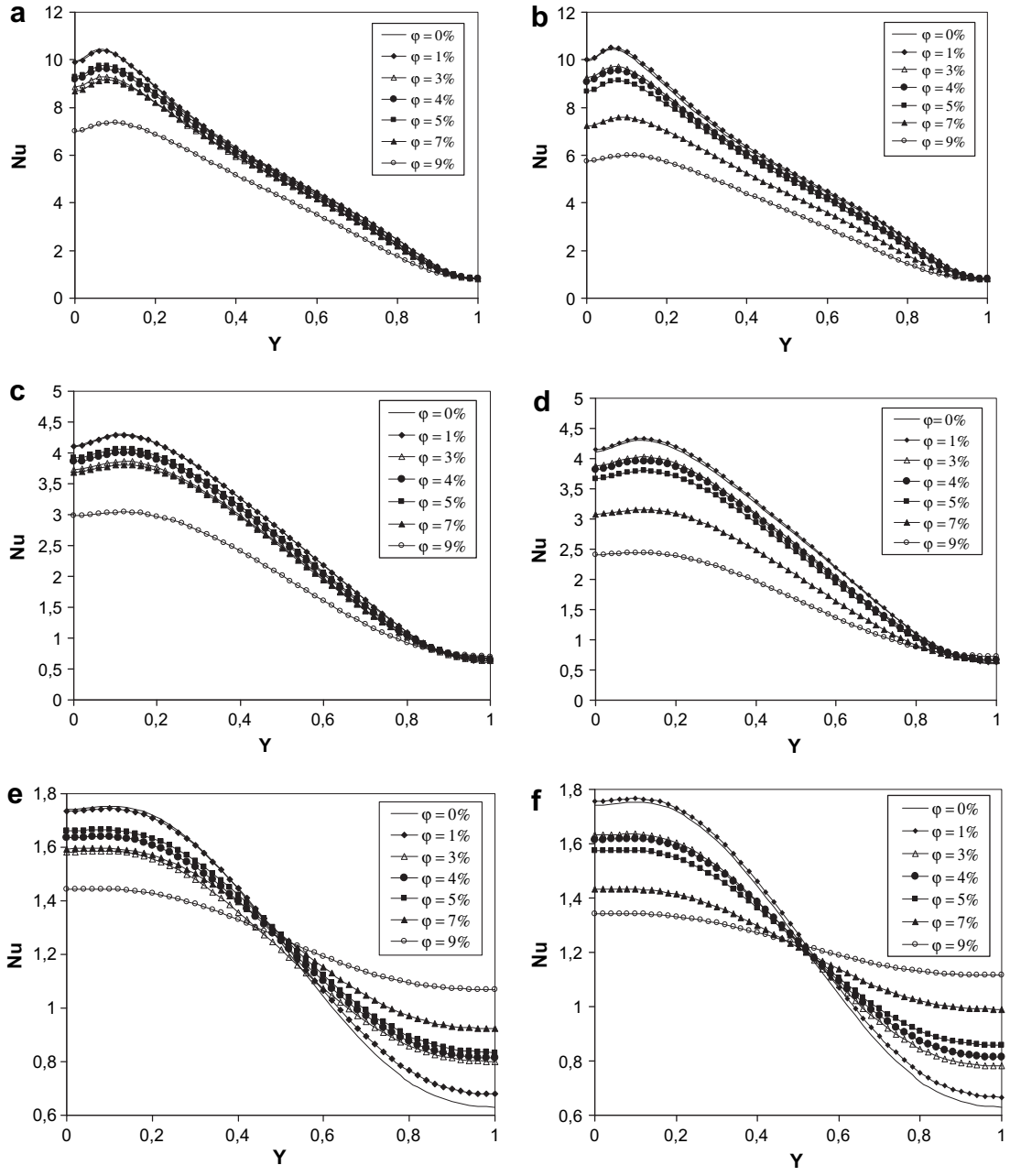

Fig. 4. Nusselt number distribution along the heated surface, $A = 1$, CuO (right column), Al_2O_3 (left column), a) $Ra = 10^5$, b) $Ra = 10^4$, c) $Ra = 10^3$, d) $Ra = 10^5$, e) $Ra = 10^4$, f) $Ra = 10^3$.

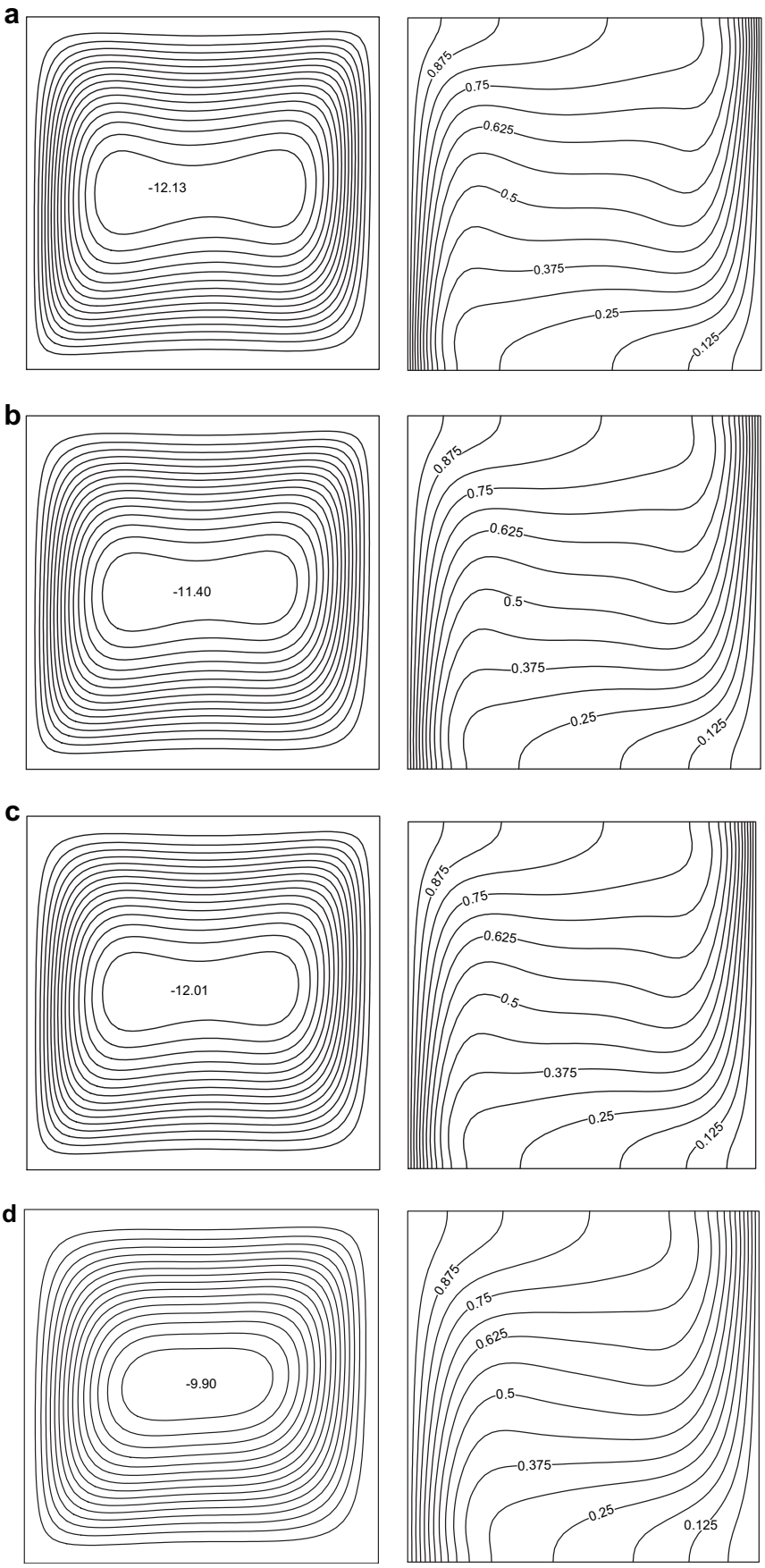

Fig. 5. Streamlines (on the left) and isotherms (on the right) for Al_2O_3–water nanofluid at $Ra = 10^5$ with different volume fractions (a) $\varphi = 1\%$, (b) $\varphi = 3\%$, (c) $\varphi = 5\%$, (d) $\varphi = 9\%$.

$$Nu = -\left(\frac{k_{nf}}{k_f}\right)\frac{\partial\theta}{\partial x} \quad (29)$$

where (k_{nf}/k_f) is calculated using Eq. (9). Finally, the average Nusselt number is determined from:

$$Nu_{avg} = \int_0^1 Nu(y)\,dy \quad (30)$$

To evaluate Eq. (30), the 1/3 Simpson's rule of integration is implemented. For convenience, a normalized average Nusselt number is defined as the ratio of Nusselt number at any volume fraction of nanoparticles to that of pure water that is:

$$*Nu_{avg}(\varphi) = \frac{Nu_{avg}(\varphi)}{Nu_{avg}(\varphi = 0)} \quad (31)$$

The average Nusselt number is used as an indicator of heat transfer enhancement where an increase in Nusselt number corresponds to an enhancement in heat transfer.

4. Grid testing and code validation

An extensive mesh testing procedure was conducted to guarantee a grid independent solution. Seven different mesh combinations were explored for the case of $Ra = 10^5$, $Pr = 0.7$. The present code was tested for grid independence by calculating the average Nusselt number on the left wall. In harmony with this, it was found that a grid size of 51×51 ensures a grid independent solution. The converged value ($Nu = 4.644$) was compared to other known values reported in the literature as shown in Table 2 and a good agreement is observed.

The present numerical solution was further validated by comparing the present code results for $Ra = 10^5$ and $Pr = 0.70$ with the experimental results of Krane and Jessee [4] and the numerical simulation of Khanafer et al. [8]. It is evident that the outcome of present code is in excellent agreement with the work reported in the literature as reflected in Fig. 3. Another grid independence study was performed using both Al_2O_3–water and CuO–water nanofluids. It was confirmed that the same grid size (51×51) ensures a grid independent solution.

5. Results and discussion

The magnitude of Rayleigh numbers, volume fractions of nanoparticles, and aspect ratios, under study here, are $Ra = 10^3$–10^5, $0 \le \varphi \le 9\%$, and $0.5 \le A \le 2$, respectively. It is worth mentioning that the right wall temperature of the enclosure is fixed to the reference temperature i.e., at 22 °C, whereas the difference between the hot and the cold wall is fixed to 30 °C, i.e., the hot wall temperature is set to 52 °C. The Prandtl number at the reference temperature is calculated as 6.57.

Fig. 4 presents the Nusselt number variation along the heated surface using various volume fractions of Al_2O_3 and CuO nanoparticles for $A = 1$. For the cases of $Ra = 10^5$ and $Ra = 10^4$, it is observable that an increase in the volume fraction of nanoparticles results in a reduced Nusselt number. This trend is always true for CuO nanoparticles. However, for Al_2O_3 with a volume fraction of 3% exhibits better enhancement than those for 4% or 5%, which is still lower than pure water. This behavior will be addressed later in this section. Fig. 5 illustrates how the thickness of the thermal boundary layer adjacent to the heated wall is influenced by the addition of nanoparticles. This sensitivity of the thermal boundary layer thickness to the volume fraction of nanoparticles is related to the increased viscosity at high volume fraction of nanoparticles (see Fig. 2). High values of φ cause the fluid to become more viscous which causes the velocity to attenuate accordingly (see Fig. 6), resulting in a reduced convection. The reduction in velocity and convection tends to increases the thermal boundary layer thickness. The growth in thermal boundary layer thickness is responsible for the lesser temperature gradients at the heated surface which lowers the Nusselt number accordingly, see Eq. (29).

Conversely, for the case of $Ra = 10^3$, the addition of nanoparticles causes the thermal boundary layer thickness to increase for $y < ½$ and to decrease for $y > ½$. This change is clearly demonstrated by the temperature isotherms in Fig. 7 where isotherms start to straighten up near the heated wall as the volume fraction of nanoparticles increases. Furthermore, for a high volume fraction of nanoparticles, say $\varphi = 9\%$, isotherms become almost parallel to the heated wall. Actually, for $\varphi = 9\%$ and $y > ½$, the isotherms become closer to the wall and for $y < ½$ the isotherms spread away from the heated wall. The isotherms exhibit a trend almost similar to conduction in solids. This behavior leads to an enhancement in heat transfer for $y > ½$ and debilitated Nusselt number for $y < ½$. This explains the behavior observed at $\varphi = 9\%$ where the Nusselt number variation along the heated surface becomes less pronounced when compared to lower volume fraction of nanoparticles as revealed in Figs. 4(c) and (f), and 7(d). Fig. 5 portrays streamlines (on the left) and isotherms (on the right) for the case of $Ra = 10^5$. It is evident that by elevating the volume fraction of nanoparticles, the maximum strength of the streamlines is attenuated due to the higher viscosity of the nanofluids, as mentioned earlier. A similar behavior is also prevalent in Fig. 7 for the case of $Ra = 10^3$.

Shown in Fig. 8 is the average Nusselt number as well as the normalized average Nusselt number along the heated surface for $A = 1$. It is observed that, for both Al_2O_3 and CuO nanoparticles, and for the case of $Ra = 10^4$ and $Ra = 10^5$, a decrease in Nusselt number occurs for volume fraction of nanoparticles greater than 5%. However, that tendency is not observed in Al_2O_3 nanofluid for a volume fraction less than 5% where fluctuations in Nusselt number are detected. In general, the influence of nanoparticles elucidates two opposing effects on the Nusselt number: a favorable effect that is driven by the presence of high thermal conductivity

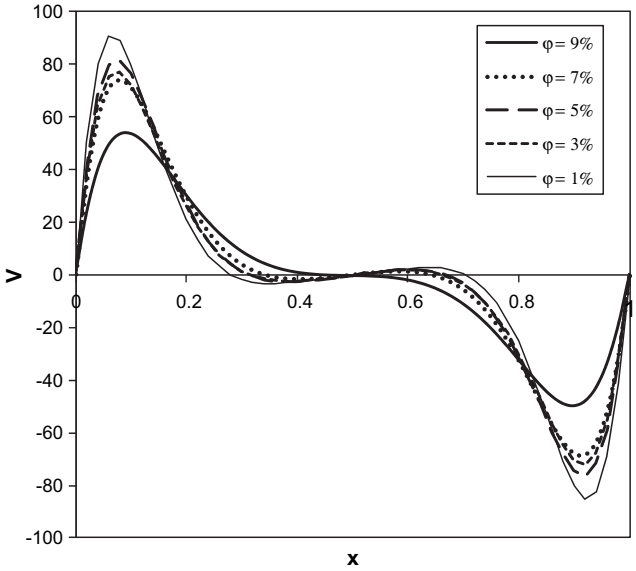

Fig. 6. Variation of y-component of velocity for $A = 1$, $y = 0.5$, $Ra = 10^5$ and Al_2O_3–water.

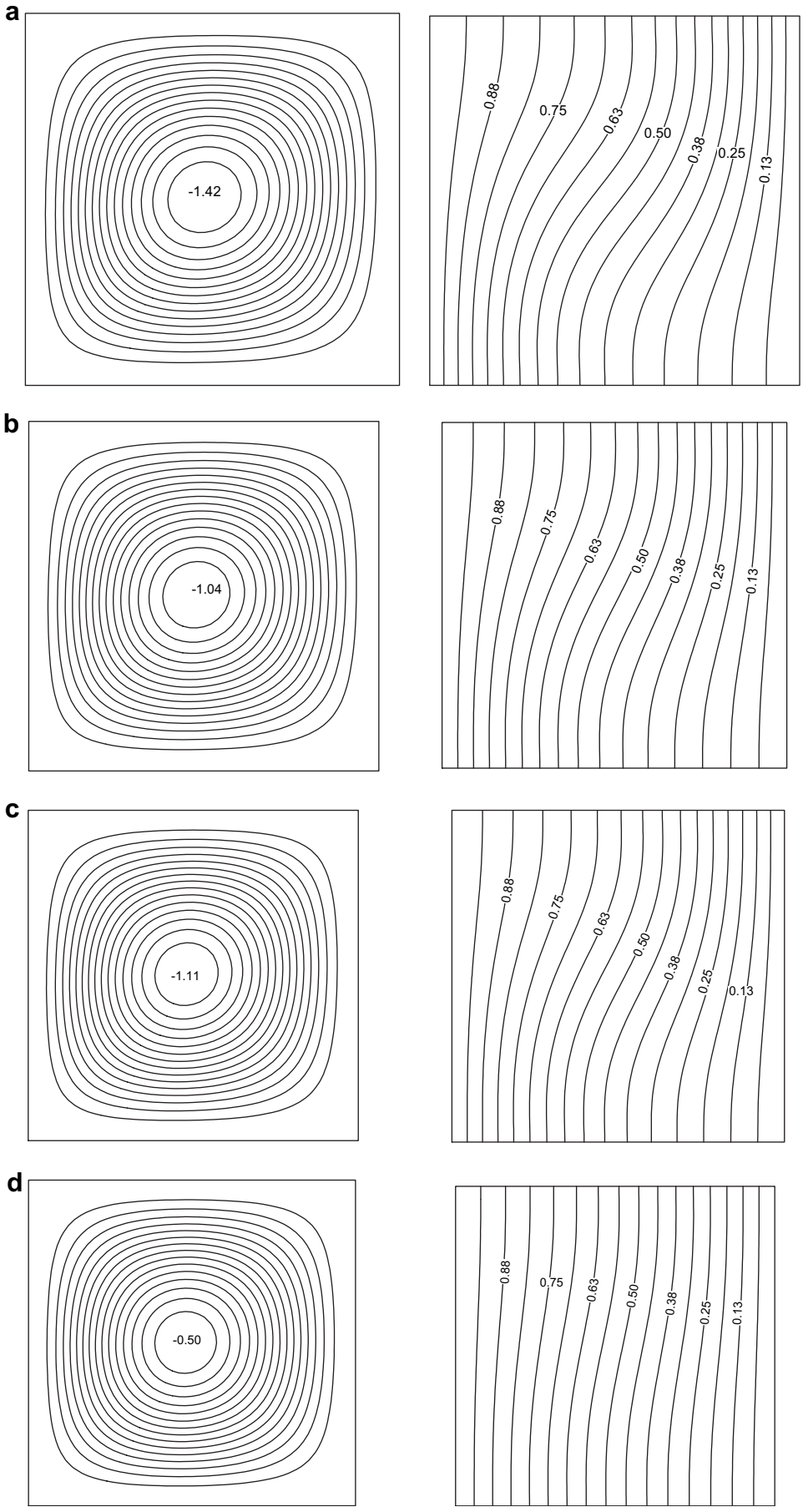

Fig. 7. Streamlines (on the left) and isotherms (on the right) for Al_2O_3–water nanofluid at $Ra = 10^3$, $A = 1$ (a) $\varphi = 1\%$, (b) $\varphi = 3\%$, (c) $\varphi = 5\%$, (d) $\varphi = 9\%$.

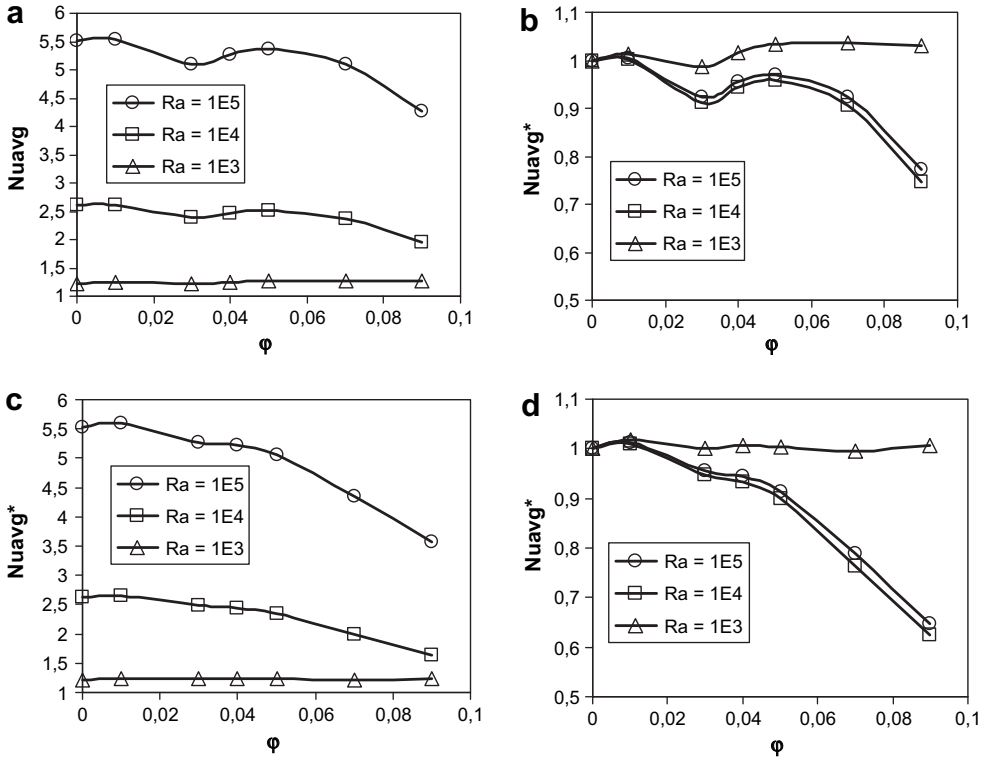

Fig. 8. (a) Average Nusselt number, $A = 1$, Al_2O_3; (b) normalized average Nusselt number, $A = 1$, Al_2O_3; (c) average Nusselt number, $A = 1$, CuO; (d) normalized average Nusselt number, $A = 1$, CuO.

nanoparticles, and an undesirable effect promoted by the high level of viscosity experienced at high volume fractions of nanoparticles. In other words, the heat transfer in natural convection at high Rayleigh numbers is dominated by convection while at low Rayleigh numbers is dominated by conduction. Therefore, for $Ra = 10^5$ and 10^4, the heat transfer dominated by convection and by the presence of nanoparticles will make the nanofluid to be more viscous, which will reduce convection currents and accordingly diminish the temperature gradient and the Nusselt number at the heated surface. This phenomenon is accompanied by some enhancement in heat transfer due to the high thermal conductivity of nanoparticles but, such enhancement is small compared to the deterioration brought by the viscosity. This is attributed to the fact that the convection currents next to the heated surface will be decelerated and the role of Brownian motion become less pronounced because the thermal conductivity of nanofluids is inversely proportional to the square of viscosity as confirmed in Eq. (13). Therefore, for high Rayleigh numbers, an adverse effect on the Nusselt number will occur for higher volume fractions of nanoparticles ($\varphi > 5$). However, for $\varphi \leq 5$, the role of viscosity is less significant and the adverse effect of viscosity is in part balanced by the beneficial effect of thermal conductivity, which explains the fluctuations in Nusselt number for $\varphi \leq 5$ using Al_2O_3.

Switching to CuO–water nanofluid, there is always a decrease in average Nusselt number since the viscosity of CuO is relatively large compared to Al_2O_3 as seen in Fig. 2. This implies that the viscosity effect dominates the favorable thermal conductivity effects. The end result is a decrease of Nusselt number by increasing the volume fraction of nanoparticles. It is also worth mentioning that the case of $Ra = 10^4$ more deterioration in Nusselt number takes place when compared to $Ra = 10^5$ case. In fact, for $Ra = 10^4$, the inertia forces are smaller than those of $Ra = 10^5$. This causes an adverse effect of nanoparticles to become more severe at $Ra = 10^4$, which leads to more reduction in Nusselt number compared to $Ra = 10^5$. On the other hand, for low Rayleigh numbers, i.e., $Ra = 10^3$, the heat transfer is dominated by conduction. Hence, by adding more nanoparticles, the conduction is enhanced due to primarily the high thermal conductivity of nanoparticles, and correspondingly the heat transfer is enhanced.

Fig. 9 illustrates how the addition of nanoparticles influences the Nusselt number distribution along the heated surface for different aspect ratios of the enclosure. The curves corroborate that for the case of $Ra = 10^5$, the behavior encountered using a low aspect ratio is similar to that for a high aspect ratio. In contrast, for $Ra = 10^4$ and 10^3, the Nusselt number is very sensitive to the aspect ratio. Comparing the values of the local Nusselt number to the case of pure fluid, it is evident that for the case of $Ra = 10^3$ the location, at which the enhancement in heat transfer is observed is shifted to $y \geq 0.6$ for $A = 2$, and to $y \geq 0$ for $A = 0.5$. This signifies almost complete enhancement all over the heated surface for $A = 0.5$ as compared to 0.4 that was provided by $A = 1$. As a consequence, the region along the heated surface where enhancement in heat transfer occurs is enlarged. This translates into an enhancement in the average Nusselt number along the heated surface as indicated in Fig. 10. Incidentally, it is interesting to note that in Fig. 9(d), for $Ra = 10^4$, there is an enhancement in Nusselt number when $y > ½$, which is not observed for other aspect ratios. Therefore, it is expected that the average Nusselt number for $Ra = 10^4$ and $A = 0.5$ decays when using higher volume fraction of nanoparticles as will be explained in Fig. 10.

Fig. 10 contains the average normalized Nusselt number using different aspect ratios. It is obvious that for $A = 2$, no enhancement in Nusselt number is observed for the full range of Rayleigh numbers. This is also demonstrated in Fig. 11 where the cases of $Ra = 10^5$ and $Ra = 10^3$ are represented to point out the significance of the aspect ratio. This pattern is antagonized with what was

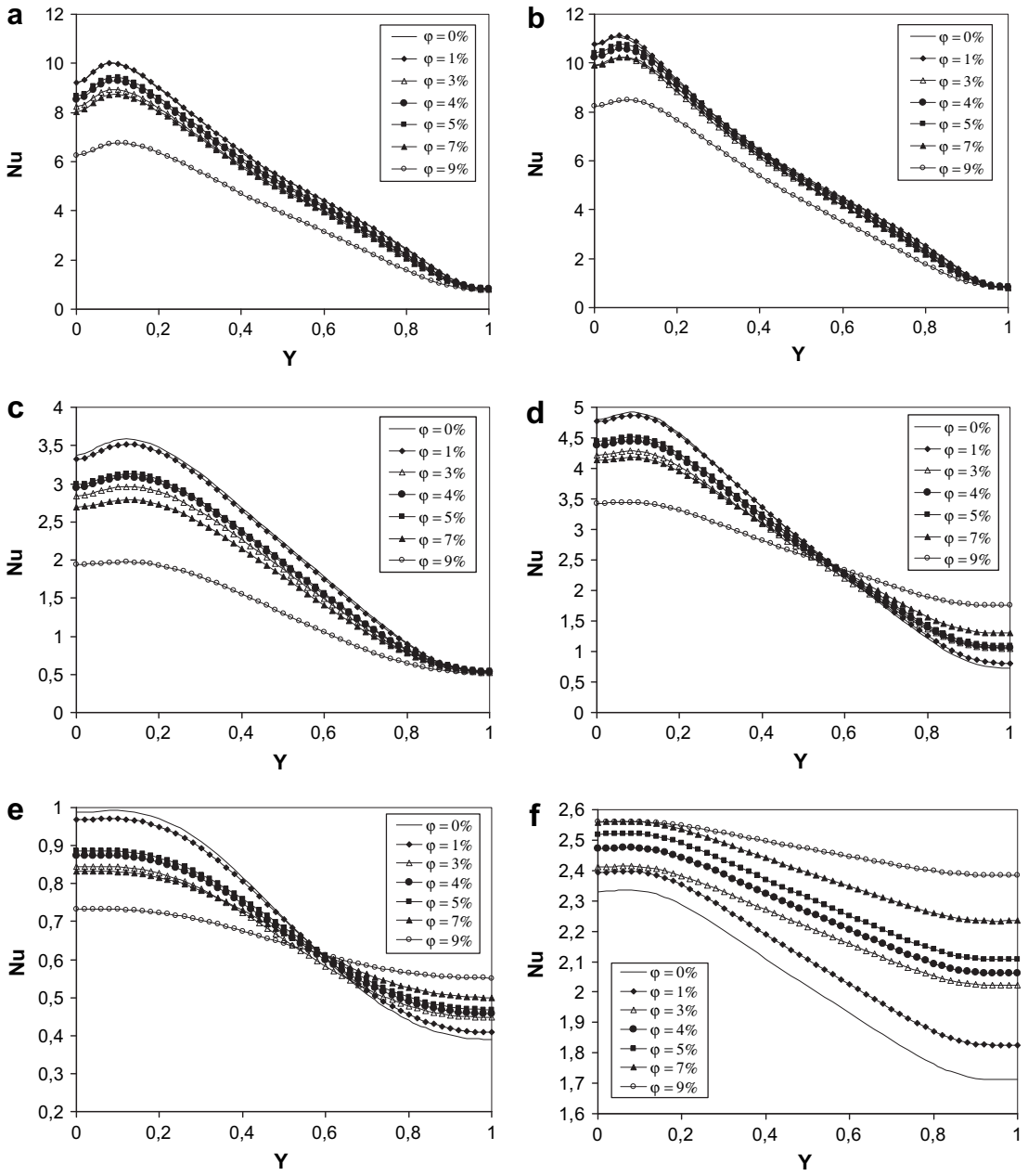

Fig. 9. Nusselt number distribution along the heated surface using Al_2O_3 nanoparticles (a) $Ra = 10^5$, $A = 2$; (b) $Ra = 10^5$, $A = 0.5$; (c) $Ra = 10^4$, $A = 2$; (d) $Ra = 10^4$, $A = 0.5$; (e) $Ra = 10^3$, $A = 2$; (f) $Ra = 10^3$, $A = 0.5$.

observed for $A = 1$, especially for $Ra = 10^3$. Moreover, it is evident that the addition of nanoparticles for $A = 2$ brings down the Nusselt number at higher rates compared to $A = 1$ using similar Rayleigh numbers. For $A = 0.5$, the enhancement in heat transfer for $Ra = 10^3$ (25%) is more pronounced when compared to $A = 1$ (5%), while a reduction is observed for $A = 2$. In the case of $A = 0.5$, the variation in average Nusselt number for $Ra = 10^4$ is very small where the maximum reduction in Nusselt number is around 10% compared to 40% for $A = 1$. This in part is related to the previous discussion connected to Fig. 9(d). It is also noted from Fig. 10 that for $A = 0.5$, both $Ra = 10^5$ and 10^4 experience exactly similar levels of enhancement. However, a bifurcation which is palpable around $\varphi = 5\%$ where the Nusselt number corresponds to $Ra = 10^5$ continues to decline at much higher rate than $Ra = 10^4$. It is concluded from Figs. 10 and 11 that high aspect ratios enclosures experience more deterioration in Nusselt number compared to low aspect ratio enclosures. In sum, enclosures with low aspect ratios would benefit from the nanoparticles thermal conductivity at low Rayleigh numbers.

Fig. 12 illustrates a comparison between the various models used for thermal conductivity and viscosity on the average Nusselt number of CuO–water nanofluid. This figure reflects results obtained using four different combinations of viscosity and thermal conductivity models as outlined by Fig. 12. As outlined in Fig. 12(a and b) it is clear that the difference between the average Nusselt number calculated using the Chon et al. model and the MG model is relatively small. However, the difference in Nusselt number when using the Nguyen et al. data and Brinkman model is much more significant. This tells that the effect of that of the thermal conductivity models is less significant than that of the viscosity models at high Rayleigh

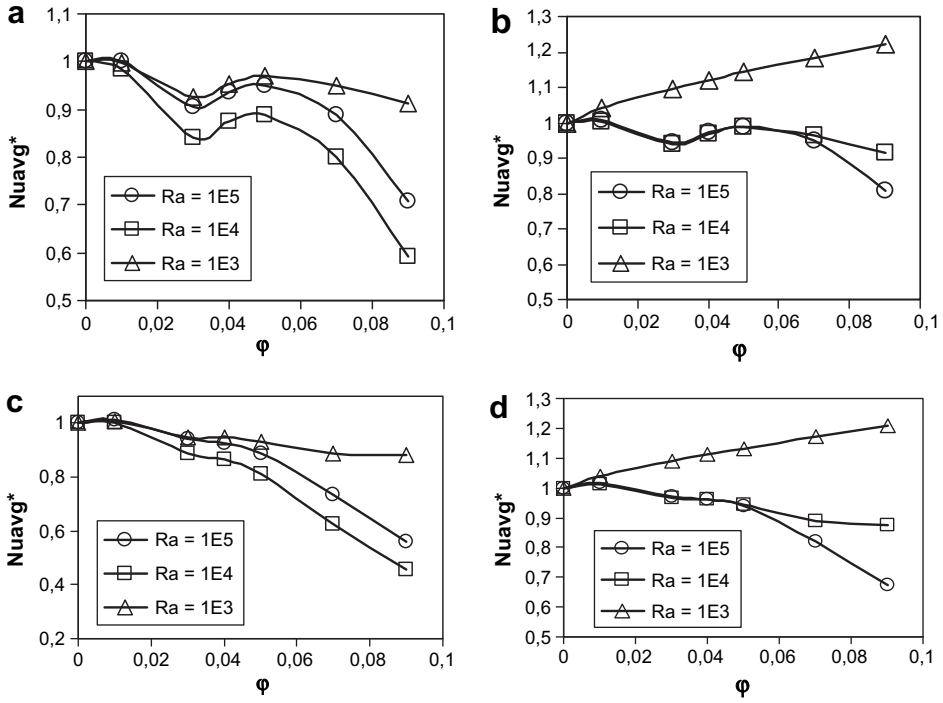

Fig. 10. Normalized average Nusselt number (a) $A = 2$, Al_2O_3; (b) $A = 0.5$, Al_2O_3; (c) $A = 2$, CuO; (d) $A = 0.5$, CuO.

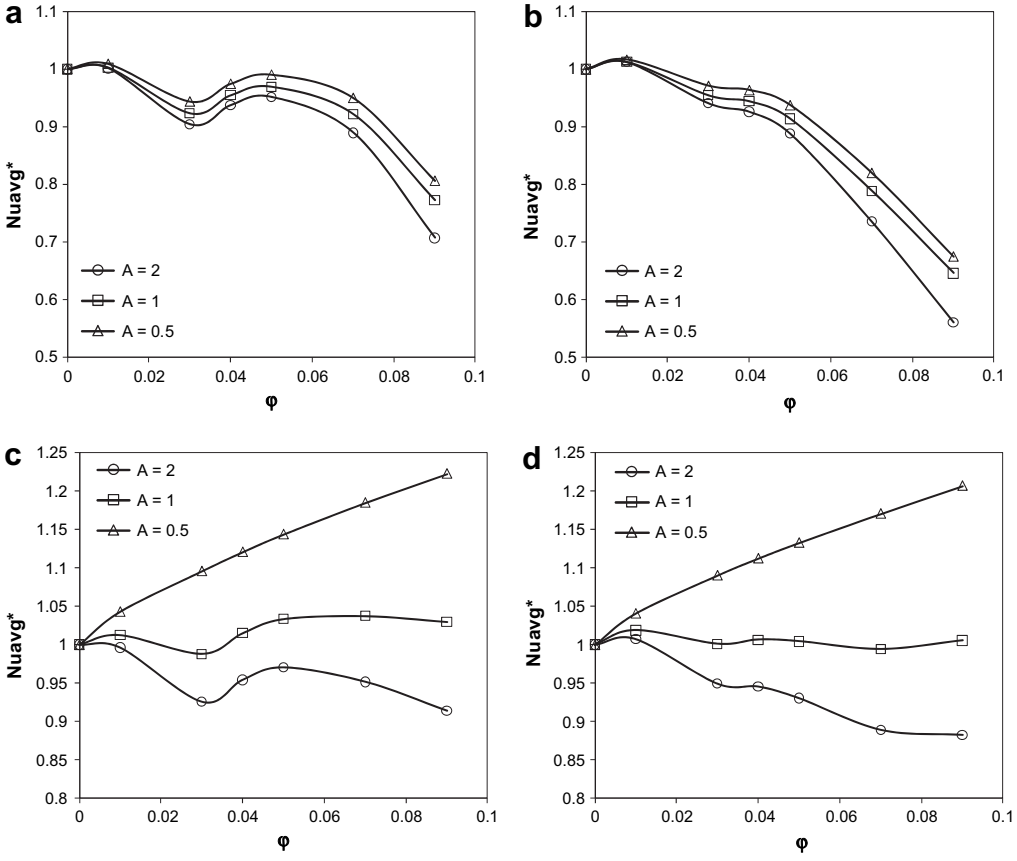

Fig. 11. Effect of aspect ratio on the normalized average Nusselt number CuO (right column), Al_2O_3 (left column) (a) $Ra = 10^5$; (b) $Ra = 10^5$; (c) $Ra = 10^3$; (d) $Ra = 10^3$.

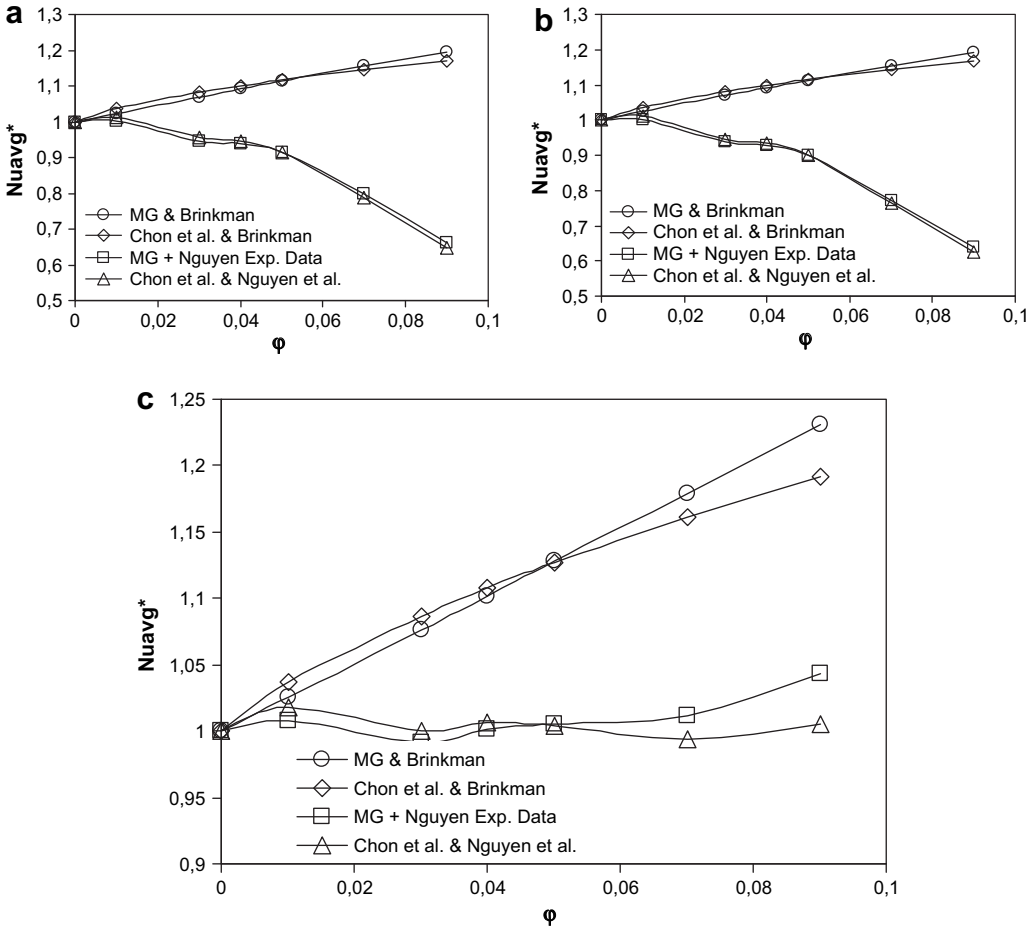

Fig. 12. Effect of the various conductivity and viscosity models on the Nusselt number, $A = 1$, CuO (a) $Ra = 10^5$; (b) $Ra = 10^4$; (c) $Ra = 10^3$.

number. As a result, the prediction of Nusselt number using the Nguyen data is completely different than that using the Brinkman model. On the other hand for low Rayleigh number, i.e., $Ra = 10^3$ when Nguyen et al. data [14] is used the Nusselt number is unrelated to volume fraction less than 6%; however, for higher volume fractions an enhancement in heat transfer is observed which is opposite to the behavior registered at high Rayleigh number (using the Nguyen et al. data). Also, Fig. 12 shows that the deviation between the Chon et al. [17] model and the MG model becomes more pronounced for $Ra = 10^3$ especially at high volume fractions of nanoparticles. Generally speaking, the MG model over predicts the enhancement in heat transfer compared to the Chon et al. model at high volume fractions of nanoparticles ($\varphi > 5\%$).

6. Conclusions

Starting with an aspect ratio equal to unity, the average Nusselt number of Al_2O_3–water nanofluid at high Rayleigh numbers is reduced by increasing the volume fraction of nanoparticles above 5%. In contrast, at low Rayleigh number, the average Nusselt number is slightly enhanced by increasing the volume fraction of nanoparticles. Focusing on CuO–water nanofluid at high Rayleigh numbers they portray a continuous decrease in average Nusselt number as the volume fraction of nanoparticles is increased. However, the average Nusselt number is not sensitive to the volume fraction at low Rayleigh number. For high Rayleigh numbers, the average Nusselt number deteriorates on the entire heated surface by increasing the volume fraction of Al_2O_3 and CuO nanoparticles. The average Nusselt number is shown to be sensitive to the aspect ratio of the enclosure. It is observed that enclosures with high aspect ratios experience more deterioration in average Nusselt number when compared to enclosures with low aspect ratios. Enclosures with low aspect ratios could benefit from the nanoparticles thermal conductivity at low Rayleigh numbers. The variable thermal conductivity and the variable viscosity models were compared to the Maxwell-Garnett model and Brinkman model. It was found that at high Rayleigh number the average Nusselt number was more sensitive to viscosity models than to the thermal conductivity models. For $Ra = 10^3$, the MG model over predicts the enhancement in heat transfer when compared to the Chon et al. model at high volume fractions of nanoparticles ($\varphi > 5\%$).

References

[1] G. De Vahl Davis, I.P. Jones, Natural convection in a square cavity: a bench mark numerical solution. Int. J. Numer. Meth. Fluids 3 (1983) 227–248.
[2] G. Barakos, E. Mistoulis, Natural convection flow in a square cavity revisited: laminar and turbulent models with wall functions. Int. J. Numer. Meth. Heat Fluid Flow 18 (1994) 695–719.
[3] T. Fusegi, J.M. Hyun, K. Kuwahara, B. Farouk, A numerical study of three-dimensional natural convection in a differentially heated cubical enclosure. Int. J. Heat Mass Transfer 34 (1991) 1543–1557.
[4] R.J. Krane, J. Jessee, Some detailed field measurements for a natural convection flow in a vertical square enclosure, in: 1st ASME-JSME Thermal Engineering Joint Conference, 1 (1983) 323–329.
[5] S.U.S. Choi, Enhancing thermal conductivity of fluids with nanoparticles. in: D.A. Siginer, H.P. Wang (Eds.), Developments and Applications of Non-Newtonian Flows, FED-Vol. 231, 1995, pp. 99–105 66.
[6] W. Daungthongsuk, S. Wongwises, A critical review of convective heat transfer nanofluids. Ren. Sust. En. Rev. 11 (2007) 797–817.
[7] V. Trisaksri, S. Wongwises, Critical review of heat transfer characteristics of nanofluids. Ren. Sust. En. Rev. 11 (2007) 512–523.

[8] K. Khanafer, K. Vafai, M. Lightstone, Buoyancy-driven heat transfer enhancement in a two-dimensional enclosure utilizing nanofluids. Int. J. Heat Mass Transfer 46 (2003) 3639–3653.
[9] H.F. Oztop, E. Abu-Nada, Numerical study of natural convection in partially heated rectangular enclosure filled with nanofluids. Int. J. Heat Fluid Flow 29 (2008) 1326–1336.
[10] N. Putra, W. Roetzel, S.K. Das, Natural convection of nano-fluids. Heat Mass Transfer 39 (2003) 775–784.
[11] D. Wen, Y. Ding, Experimental investigation into convective heat transfer of nanofluids at the entrance region under laminar flow conditions. Int. J. Heat Mass Transfer 47 (2004) 5181–5188.
[12] E. Abu-Nada, Z. Masoud, A. Hijazi, Natural convection heat transfer enhancement in horizontal concentric annuli using nanofluids. Int. Commun. Heat Mass Transfer 35 (5) (2008) 657–665.
[13] B.C. Pak, Y.I. Cho, Hydrodynamic and heat transfer study of dispersed fluids with submicron metallic oxide particles. Exp. Heat Transfer 11 (1998) 151–170.
[14] C.T. Nguyen, F. Desgranges, G. Roy, N. Galanis, T. Mare, S. Boucher, H. Angue Minsta, Temperature and particle-size dependent viscosity data for water-based nanofluids – hysteresis phenomenon. Int. J. Heat Fluid Flow 28 (2007) 1492–1506.
[15] G. Polidori, S. Fohanno, C.T. Nguyen, A note on heat transfer modeling of Newtonian nanofluids in laminar free convection. Int. J. Therm. Sci. 46 (2007) 739–744.
[16] H. Angue Minsta, G. Roy, C.T. Nguyen, D. Doucet, New temperature and conductivity data for water-based nanofluids. Int. J. Therm. Sci. 48 (2) (2009) 363–371.
[17] C.H. Chon, K.D. Kihm, S.P. Lee, S.U.S. Choi, Empirical correlation finding the role of temperature and particle size for nanofluid (Al_2O_3) thermal conductivity enhancement. Appl. Phys. Lett. 87 (2005) 153107.
[18] E. Abu-Nada, Effect of variable viscosity and thermal conductivity of Al2O3–water nanofluid on heat transfer enhancement in natural convection, Int. J. Heat Fluid Flow 30 (2009) 679–690.
[19] S.P. Jang, S.U.S. Choi, Effects of various parameters on nanofluid thermal conductivity. ASME J. Heat Transfer 129 (2007) 617–623.
[20] S.V. Patankar, Numerical Heat Transfer and Fluid Flow. Hemisphere Publishing Corporation, Taylor and Francis Group, New York, 1980.
[21] H.K. Versteeg, W. Malalasekera, An Introduction to Computational Fluid Dynamic: The Finite Volume Method. John Wiley, New York, 1995.